Available online at www.sciencedirect.com
ScienceDirect
Fluid Dynamics Research 40 (2008) 637–661
FLUID DYNAMICS RESEARCH

Modified incompressible SPH method for simulating free surface problems

B. Ataie-Ashtiani*, G. Shobeyri[1], L. Farhadi

Department of Civil Engineering, Sharif University of Technology, Tehran, Iran

Received 19 March 2006; received in revised form 17 July 2007; accepted 12 December 2007
Available online 22 January 2008
Communicated by M. Oberlack

Abstract

An incompressible smoothed particle hydrodynamics (I-SPH) formulation is presented to simulate free surface incompressible fluid problems. The governing equations are mass and momentum conservation that are solved in a Lagrangian form using a two-step fractional method. In the first step, velocity field is computed without enforcing incompressibility. In the second step, a Poisson equation of pressure is used to satisfy incompressibility condition. The source term in the Poisson equation for the pressure is approximated, based on the SPH continuity equation, by an interpolation summation involving the relative velocities between a reference particle and its neighboring particles. A new form of source term for the Poisson equation is proposed and also a modified Poisson equation of pressure is used to satisfy incompressibility condition of free surface particles. By employing these corrections, the stability and accuracy of SPH method are improved. In order to show the ability of SPH method to simulate fluid mechanical problems, this method is used to simulate four test problems such as 2-D dam-break and wave propagation.

Keywords: Incompressible flow; Numerical method; Lagrangian method; Dam-break

* Corresponding author.
E-mail addresses: ataie@sharif.edu (B. Ataie-Ashtiani), shobeyri@iust.ac.ir (G. Shobeyri).
[1] Now Ph.D. student at Iran University of Science and Technology.

0169-5983/$32.00
doi:10.1016/j.fluiddyn.2007.12.001

1. Introduction

Free surface hydrodynamic flows are of significant industrial and environmental importance. These problems are difficult to simulate due to the existence of the arbitrarily moving surface boundary conditions and also because of the complex governing equations of Navier–Stokes (N–S). The marker and cell (Harlow and Welch, 1965) and volume of fluid (Hirt and Nichols, 1981; Sussman, 2003) methods are two of the most flexible and powerful models for simulating such flows, in which the N–S equations are solved on a fixed Eulerian grid. In the former, marker particles are used to define free surface while in the latter governing equations are solved for the volume fraction of the fluid. They have been successfully applied to a wide variety of flow problems involving free surfaces but they remain complicated to program. Also in spite of successful use of both methods for treating free surface flows, numerical diffusion due to solving N–S equations on a fixed Eulerian grid arise especially when the deformation of free surface is very large (Shao and Lo, 2003).

Recently particle methods have been used in which each particle is followed in a Lagrangian manner. Moving interfaces and boundaries can be analyzed by mesh-less methods much easier than mesh-base methods. Furthermore in Lagrangian formulations, the convection terms are calculated without any numerical diffusion (Ataie-Ashtiani and Farhadi, 2006; Farhadi and Ataie-Ashtiani, 2004a, b).

Different particle methods have been proposed and developed over the recent years. The first idea was proposed by Gingold and Monaghan (1977) for the treatment of astrophysical hydrodynamic problems with the method called smoothed particle hydrodynamics (SPH) in which kernel approximations are used to interpolate the unknowns. This method was later generalized to fluid mechanic problems (Monaghan, 1994).

Two different approaches can be used to extend SPH method to nearly incompressible or incompressible flows. In the first approach, real fluids are treated as compressible fluids (Monaghan, 1994). This artificial compressibility can cause problems with sound wave reflection at boundaries and high sound speed leads to a stringent CFL time step constraint (Shao and Lo, 2003). On the other hand, because of explicit computation to estimate pressure of particles by a stiff equation of state, this approach leads to a lower computational costs and also it has proved to be an effective method in tracking free surface problems (Monaghan, 1994, 1996; Monaghan and Kos, 1999). The second approach works directly with the constraint of constant density and employs a strict incompressibility conditions for fluids (Lo and Shao, 2002; Shao and Lo, 2003; Shao and Gotoh, 2005). Unlike compressible SPH, in incompressible SPH method (I-SPH) the pressure is directly obtained by solving a Poisson equation of pressure that satisfies incompressibility.

SPH method has been shown to be applicable to a wide range of problems such as wave propagation (Monaghan and Kos, 1999; Shao and Gotoh, 2005), gravity currents (Monaghan, 1996), free surface Newtonian and non-Newtonian flows (Shao and Lo, 2003) and wave impact on tall structures (Gomez-Gesteria and Dalrymple, 2004).

A similar approach is the moving particle semi-implicit (MPS) method proposed by Koshizuka and Oka (1996). In this case, motion of each particle is calculated through interactions with neighboring particles using an approximate kernel (weight) function. Laplacian, gradient and divergence operators are transformed to interaction among moving particles. This method has been applied in the hydrodynamics and nuclear mechanics field such as the study of dam-breaking (Ataie-Ashtiani and Farhadi, 2006; Koshizuka and Oka, 1996), wave breaking (Koshizuka et al., 1998) and vapor explosion (Koshizuka et al., 1999). Various kernel functions and different methods of solving the Poisson equation of pressure

were considered and applied to improve the stability and accuracy of MPS method (Ataie-Ashtiani and Farhadi, 2006).

In this paper, some modifications for the conventional I-SPH method applied for incompressible flows are presented. A new form of source term for the Poisson equation of pressure and a modified Poisson equation of pressure, enforcing incompressibility condition to free surface particles, are proposed. These modifications considerably improve the stability and accuracy of the incompressible SPH method. Ataie-Ashtiani and Shobeiry (2008) have also applied the present method for the numerical simulation of landslide impulsive waves.

2. SPH formulation

2.1. Interpolation

The SPH formulation is obtained as a result of interpolation between a set of disordered points known as particles. The interpolation is based on the theory of integral interpolants that uses kernel function to approximate delta function. Each particle carries a mass [M], a velocity [LT^{-1}] and all the properties of fluid with it. The key idea in this method is to consider that a function $A(r)$ can be approximated by (Liu, 2003):

$$A(\vec{r}_a) = \sum_b m_b \frac{A_b}{\rho_b} W(|\vec{r}_a - \vec{r}_b|, h). \tag{1}$$

Thus by summing over the particles the fluid density at particle a, ρ_a [ML^{-3}], is evaluated according to the following equation:

$$\rho_a = \sum_b m_b W(|\vec{r}_a - \vec{r}_b|, h), \tag{2}$$

where a is the reference particle and b is its neighboring particle. m_b [M] and ρ_b [ML^{-3}] are mass and density, respectively, W is interpolation kernel, h [L] is smoothing distance which determines width of kernel and ultimately the resolution of the method.

Based on Eq. (2), we can deduce that the density of particle a increases when particle b is getting closer to it.

2.2. Kernel (weight) function

Kernel (weight) functions should have specific properties such as positivity, compact support, unity, monotonically decreasing and delta function behavior (Liu, 2003). These properties are represented in the following equation:

$$\begin{array}{ll} W(r,h) > 0 \ \text{ over } \Omega & \text{positivity,} \\ W(r,h) = 0 \ \text{ outside } \Omega & \text{compact,} \\ \int_\Omega W(r,h) \cdot \mathrm{d}r = 1 & \text{unity,} \\ W \text{ is monotonically decreasing function} & \text{decay,} \\ W(r,h) \to \delta \ \text{ as } h \to 0 & \text{delta function behavior,} \end{array} \tag{3}$$

where r [L] is distance between particles, $q = r/h$ and Ω is the support domain.

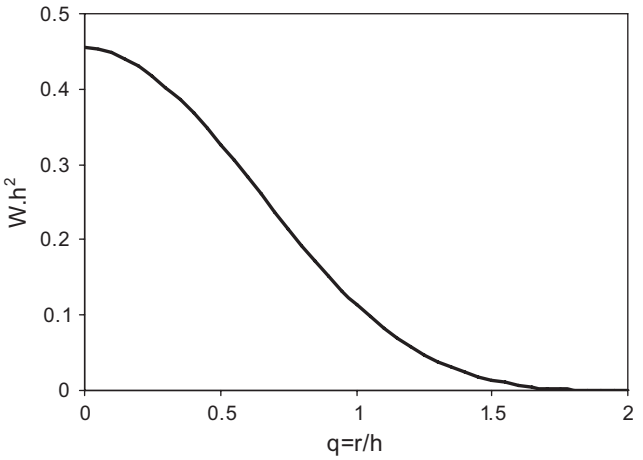

Fig. 1. Kernel shape of the spline function.

Many different kernel functions satisfying the required conditions have been proposed by researchers. Monaghan (1992) introduced a kernel function which has a spline form in 2-D described as:

$$\begin{aligned} W(r,h) &= \frac{10}{7\pi h^2}\left(1-\frac{3}{2}q^2+\frac{3}{4}q^3\right), \quad q<1,\\ W(r,h) &= \frac{10}{28\pi h^2}(2-q)^3, \qquad 1\leqslant q\leqslant 2,\\ W(r,h) &= 0, \qquad q>2. \end{aligned} \tag{4}$$

The shape of this kernel function is shown in Fig. 1.

Since the size of the area covered by the weight function around particle a is limited, the particle interacts with a finite number of neighboring particles. If the weight function is not limited, the operation count is the scale of N^2 where N is the total number of particles (Koshizuka and Oka, 1996).

2.3. Gradient model

The gradient term in the N–S equation can have different forms in SPH formulation. A model of gradient that preserves linear and angular momentum is (Monaghan, 1994):

$$\left(\frac{1}{\rho}\nabla P\right)_a = \sum_b m_b\left(\frac{P_a}{\rho_a^2}+\frac{P_b}{\rho_b^2}\right)\nabla_a W_{ab}. \tag{5}$$

2.4. Laplacian model

Laplacian involves the second derivative of the kernel function that is very sensitive to particle disorder (Shao and Lo, 2003). In Laplacian of pressure this can cause pressure instability. Thus developing a

model of Laplacian, which prevents this instability, is very important. Lo and Shao (2002) used a model of Laplacian that has this specific characteristic and is stable.

$$\nabla \cdot \left(\frac{1}{\rho}\nabla P\right)_a = \sum_b m_b \frac{8}{(\rho_a + \rho_b)^2} \frac{P_{ab}\vec{r}_{ab} \cdot \nabla_a W_{ab}}{|\vec{r}_{ab}|^2 + \eta^2}, \tag{6}$$

where P_{ab} $[\mathrm{ML}^{-1}\mathrm{T}^{-2}] = P_a - P_b$, $\vec{r}_{ab}[\mathrm{L}] = \vec{r}_a - \vec{r}_b$ and $\eta[\mathrm{L}] = 0.1\,\mathrm{h}$.

The corresponding coefficient matrix of the linear equations (Eq. (6)) is scalar, symmetric and positive definite and can be more efficiently solved by an iterative scheme.

3. Mathematical and numerical formulation

The governing equations of non-viscous fluid flows which are mass and momentum conservation are presented in the following equations, respectively.

$$\frac{1}{\rho}\frac{\mathrm{D}\rho}{\mathrm{D}t} + \nabla \cdot \vec{u} = 0, \tag{7}$$

$$\frac{\mathrm{D}\vec{u}}{\mathrm{D}t} = -\frac{1}{\rho}\nabla P + \vec{g}, \tag{8}$$

where ρ is density, u $[\mathrm{LT}^{-1}]$ is velocity vector, P is pressure and g $[\mathrm{LT}^{-2}]$ is gravitational acceleration.

The computation of the I-SPH method is composed of two basic steps. The first step is the prediction one in which the velocity field is computed without enforcing incompressibility. In the second step, which is called the correction step, incompressibility is enforced in the calculations through Poisson equation of pressure.

I-SPH method can be summarized in a simple algorithm combined of five stages (Shao and Lo, 2003):

(a) Initialize fluid: $\vec{r}_0, \vec{u}_0$.

For each time step:

(b) Compute forces by considering only gravitational term in Eq. (8). Apply them to particles and find temporary particle positions and velocities: $\vec{u}_*, \vec{r}_*$

$$\Delta\vec{u}_* = \vec{g}\Delta t, \tag{9}$$

$$\vec{u}_* = \vec{u}_t + \Delta\vec{u}_*, \tag{10}$$

$$\vec{r}_* = \vec{r}_t + \vec{u}_*\Delta t, \tag{11}$$

where $\vec{u}_t, \vec{r}_t$ = particle velocity and position at time t; $\vec{u}_*, \vec{r}_*$ = temporary particle velocity and position, respectively; $\Delta\vec{u}_*$ = change in the particle velocity during the prediction step.

Incompressibility is not satisfied in this step and the fluid density ρ_* that is calculated based on the temporary particle positions (Eq. (2)) deviates from the constant density ρ_0.

(c) The correction step; in this step the pressure term, obtained from the mass conservation (Eq. (7)), is used to enforce incompressibility in the calculation (Lo and Shao, 2002).

$$\frac{1}{\rho_0}\frac{\rho_0-\rho_*}{\Delta t}+\nabla\cdot(\Delta\vec{u}_{**})=0, \tag{12}$$

$$\Delta\vec{u}_{**}=\frac{-1}{\rho_*}\nabla P_{t+1}\Delta t, \tag{13}$$

$$\vec{u}_{t+1}=\vec{u}_*+\Delta\vec{u}_{**}. \tag{14}$$

By combining Eqs. (12) and (13):

$$\nabla\cdot\left(\frac{1}{\rho_*}\nabla P_{t+1}\right)=\frac{\rho_0-\rho_*}{\rho_0\Delta t^2}. \tag{15}$$

After employing the relevant SPH formulation Eq. (6) for the Laplacian operator, a system of linear equations is obtained and solved efficiently by available solvers.

(d) New particle velocities are computed by Eqs. (13) and (14).
(e) Finally, the new position of particles is centered in time.

$$\vec{r}_{t+1}=\vec{r}_t+\frac{\vec{u}_{t+1}+\vec{u}_t}{2}\Delta t, \tag{16}$$

where $\vec{r}_{t+1}, \vec{r}_t$ = position of particle at time t_{t+1} and t.

4. Boundary conditions

4.1. Wall boundaries

Solid boundaries are represented by one line of particles. The Poisson equation of pressure is solved on these particles. This balances the pressure of inner fluid particles and prevents them from accumulating in the vicinity of solid boundaries. In addition, in order to ensure that particle density number is computed accurately and wall particles are not considered as free surface particles (Koshizuka and Oka, 1996), several lines of dummy particles should be placed outside of wall boundaries.

There are at least two methods to place the dummy particles. In the first method, they are fixed in space. In the second method, image particles that mirror the physical properties of inner fluid particles are used (Lo and Shao, 2002).

In this study, we used the first method for placing dummy particles and employed a smoothing length of $h = 1.2 * L_0$ (L_0 = initial spacing between particles). Thus two layers of dummy particles were placed outside the solid boundaries. The pressure of a dummy particle is set to that of a wall particle in the normal direction of the solid walls (Shao and Lo, 2003).

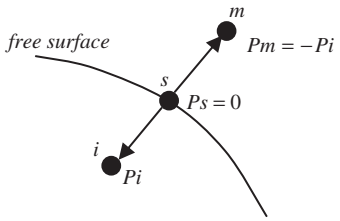

Fig. 2. Free surface boundary treatment relationship between inner, mirror and free surface particles.

4.2. Free surface

Since there are no particles in the outer region of free surface, the particle density decreases on this boundary. A particle that satisfies Eq. (17) is considered to be on free surface. In this equation β is the free surface parameter.

$$\rho_* < \beta\rho_0. \tag{17}$$

Most SPH formulations are presented in symmetric form. The symmetric particle configuration is violated on the free surface and density falls discontinuously. This leads to a spurious pressure gradient (Shao and Lo, 2003). To avoid this problem, special treatments should be considered when computing gradient operator for free surface particles. Let us assume that s is a surface particle with zero pressure and i is an inner fluid particle with pressure P_i. In order to calculate the pressure gradient between these two particles, a mirror particle with pressure $-P_i$ should be placed in the direct reflection position of inner particle i through the surface particle s. In this way, the zero pressure condition on the free surface is satisfied (see Fig. 2).

The gradient of the pressure between a free surface particle (s), a mirror particle (m) and an inner particle i is expressed as:

$$\left(\frac{1}{\rho}\nabla P\right)_{si} = m\left(\frac{P_s}{\rho_s^2} + \frac{P_i}{\rho_i^2}\right)\nabla_s W_{si} + m\left(\frac{P_s}{\rho_s^2} + \frac{P_m}{\rho_m^2}\right)\nabla_s W_{sm}, \tag{18}$$

$$P_m = -P_i,$$

$$P_s = 0,$$

$$\nabla_s W_{sm} = -\nabla_s W_{si}, \tag{19}$$

where m is a mirror, s is a surface and i is an inner particle.

Combining Eqs. (18) and (19) gives

$$\left(\frac{1}{\rho}\nabla P\right)_{si} = 2m\left(\frac{P_i}{\rho_i^2}\right)\nabla_s W_{si}. \tag{20}$$

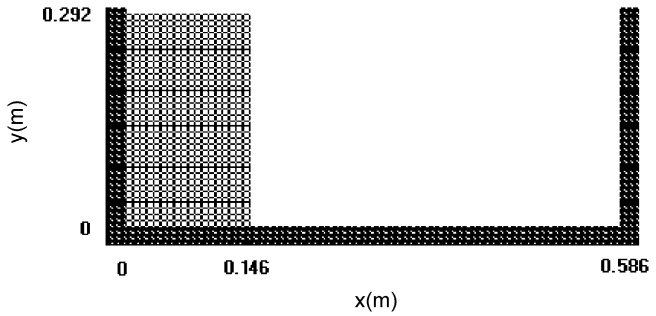

Fig. 3. Geometry of the collapse of water column.

5. Courant number condition

Since the I-SPH is a semi-implicit method (explicit in computing the convective term and implicit in computing the pressure gradient term in the momentum equation), the sizes of time steps must be controlled in order to get stable and accurate results. The computation time must satisfy the following Courant condition:

$$\Delta t \leqslant 0.1 \frac{L_0}{V_{\max}}, \tag{21}$$

where L_0 [L] is the initial particle spacing and $V_{\max}$ [LT^{-1}] is maximum particle velocity in the computation The factor 0.1 ensures that the particle moves only a fraction of the particle spacing per time step (Shao and Lo, 2003).

6. Model application

6.1. Breaking dam analysis

An idealized 2-D dam-break problem is simulated in the present section. The dam-break flow can be simulated by instantaneous removal of a barrier holding a body of water at rest. The schematic of the problem is shown in Fig. 3. Water column is represented by 648 particles which are located like a square grid. The distance between two neighboring particles (L_0) is 0.008 m. The left, right and bottom walls are represented by 474 particles. Their coordinates are fixed, and velocities are zero over time. In the computations, time step and smoothing length are 0.001 s and 0.0096 m, respectively.

As seen in Fig. 4, I-SPH method successfully simulates the collapse of water column till 1 s, but the shape of the free surface is not consistent with the experimental results of Koshizuka and Oka (1996) after 0.3 s. Particles are dispersed after the water impinges the right vertical wall at 0.3 s and the free surface shape is not satisfactory.

In I-SPH incompressibility condition is not controlled for free surface particles directly. In other words, pressure Poisson equation (Eq. (15)) is not solved on these particles and simply zero pressure is set for these particles. It is more physical if incompressibility condition is imposed on free surface particles. In

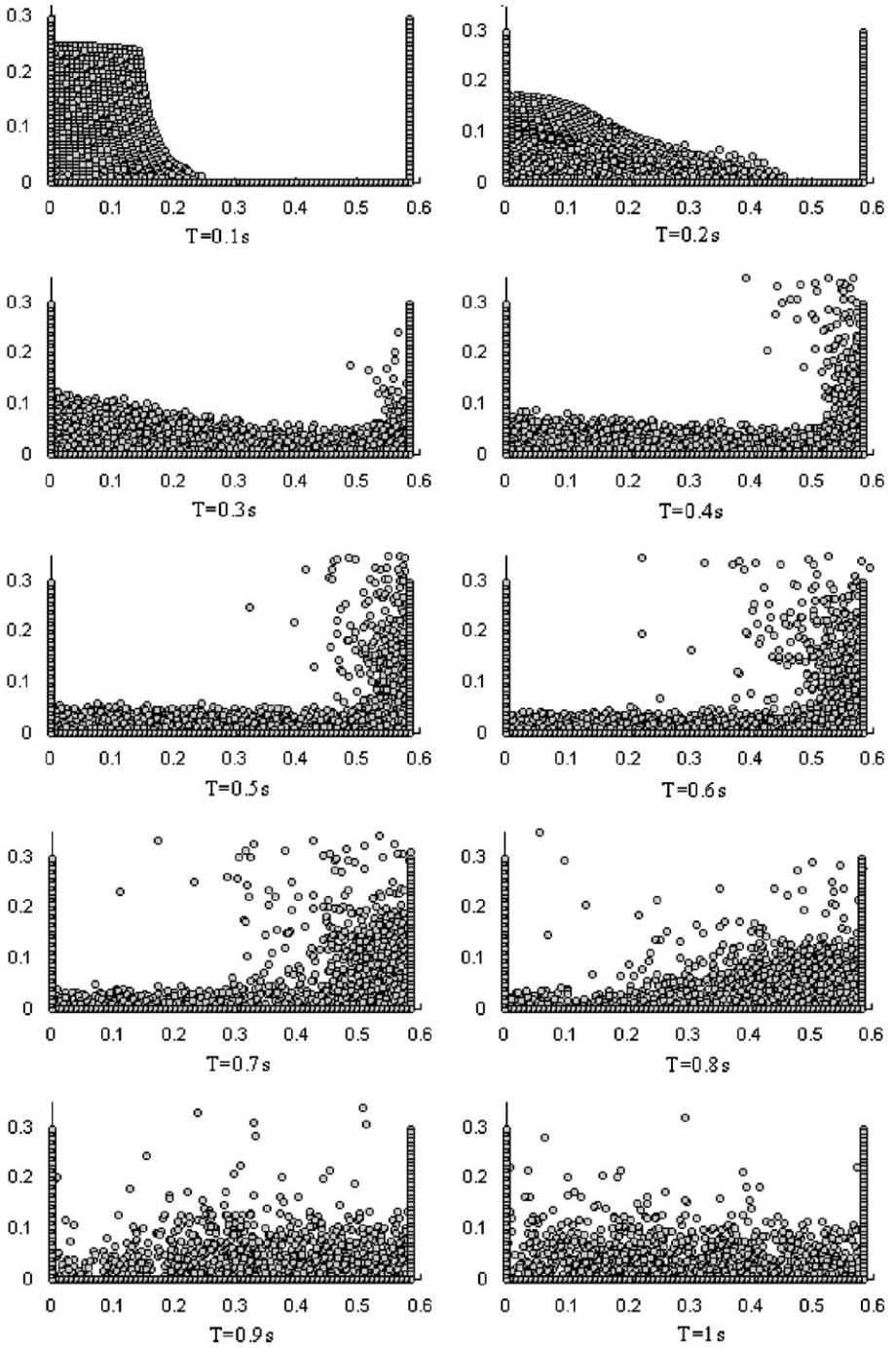

Fig. 4. Numerical simulation of collapse of water column at different times using I-SPH method (horizontal and vertical scales units are meter).

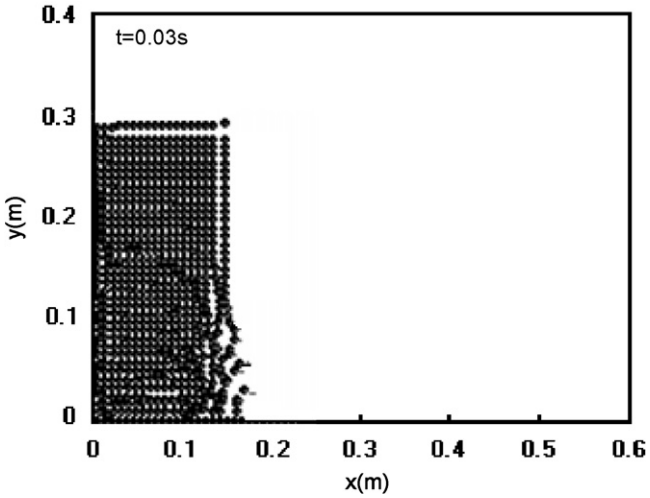

Fig. 5. Numerical simulation of collapse of water column at $t = 0.03$ s using I-SPH method to satisfy incompressibility for free surface particles.

Fig. 5 the dam-break problem is solved employing pressure Poisson equation to satisfy incompressibility of free surface particles. It is clear from the figure that the results become instable very fast. The most important reason causing instability is that there are no particles in outer region of free surface, causing spurious pressure Laplacian for free surface particles using Eq. (6). In I-SPH method, pressure gradient of free surface particles is considered to be twice of the computed value using Eq. (20) instead of Eq. (5). Employing the same procedure for the Laplacian operator:

$$\nabla \cdot \left(\frac{1}{\rho}\nabla P\right)_{si} = 2\left(m_s \frac{8}{(\rho_s + \rho_i)^2} \frac{P_{si}\vec{r}_{si} \cdot \nabla_s W_{si}}{|\vec{r}_{si}|^2 + \eta^2}\right), \tag{22}$$

where s and i are free surface and inner particle, respectively.

The Laplacian term is computed for free surface particles properly using the above equation.

6.1.1. Density error analysis for the dam-break problem

Although I-SPH is a robust approach to solve N–S equations with the incompressibility assumption but because of the errors generated due to the discretization of the governing equations, imposing boundary conditions and also solving the linear equations, completely satisfying incompressibility is impossible. At each time step, a little amount of density errors is generated and during computations accumulated.

If density of a single particle denoted with a at time $t = 0$ is ρ_0, due to the above-mentioned errors the density of this particle at time t will be:

$$\rho_0 = \rho_a^t + \Delta\rho_a^t, \tag{23}$$

where ρ_a^t, $\Delta\rho_a^t$ are density of particle a and density error until time t, respectively. At time t and the prediction step, the temporary density of the particle is shown with ρ_*. At the correction step after

including the gradient pressure term in Eq. (8):

$$\rho_a^{t+1} = \rho_* + \Delta\rho_*, \tag{24}$$

$$\rho_0 = \rho_a^{t+1} + \Delta\rho_a^{t+1}. \tag{25}$$

By combining Eqs. (24) and (25):

$$\rho_0 = \rho_* + \Delta\rho_* + \Delta\rho_a^{t+1}, \tag{26}$$

where $\Delta\rho_*$ is the deviation of density due to not including pressure term in Eq. (8) at the prediction step.

In I-SPH method, the source term of the Poisson equation (Eq. (15)) for the particle is computed by

$$\frac{\rho_0 - \rho_*}{\rho_0 \Delta t^2} = \frac{\Delta\rho_* + \Delta\rho_a^{t+1}}{\rho_0 \Delta t^2}. \tag{27}$$

In the source term only $\Delta\rho_*$ should contribute but in I-SPH both parts of $\Delta\rho_*$ and $\Delta\rho_a^{t+1}$ are considered. In our work a modification in this regard has been applied by including only $\Delta\rho_*$ in the source term. This means that the previous density errors are not allowed to affect the source term.

Changes in the fluid density can be computed through:

$$\frac{\mathrm{d}\rho_a}{\mathrm{d}t} = \sum_b m_b \frac{\mathrm{d}(W_{ab})}{\mathrm{d}t}. \tag{28}$$

And also changes in the values of the kernel function:

$$\frac{\mathrm{d}W(x_{ab}, y_{ab})}{\mathrm{d}t} = \left(\frac{\partial W_{ab}}{\partial x} \cdot \frac{\mathrm{d}x_{ab}}{\mathrm{d}t} + \frac{\partial W_{ab}}{\partial y} \cdot \frac{\mathrm{d}y_{ab}}{\mathrm{d}t} \right) = \vec{\nabla}_a W_{ab} \cdot \vec{u}_{ab}, \tag{29}$$

where $\vec{u}$ is velocity and $\vec{u}_{ab} = \vec{u}_a - \vec{u}_b$.

Change in the density of the particle at the prediction step is

$$\frac{\Delta\rho_*}{\rho_0 \Delta t^2} = \frac{1}{\rho_0 \mathrm{d}t} \frac{\mathrm{d}\rho}{\mathrm{d}t}. \tag{30}$$

By combining Eqs. (28) and (30), the new source term is described with:

$$\frac{1}{\rho_0 \mathrm{d}t} \sum_b m_b (\vec{u}_a - \vec{u}_b) \cdot \vec{\nabla}_a W_{ab}. \tag{31}$$

And finally the pressure Poisson equation is described as:

$$\vec{\nabla} \cdot \left(\frac{1}{\rho_*} \vec{\nabla} P_{t+1} \right) = \frac{1}{\rho_0 \mathrm{d}t} \sum_b m_b (\vec{u}_a - \vec{u}_b) . \vec{\nabla}_a W_{ab}. \tag{32}$$

The same procedure can be used for all particles.

In this form of Poisson equation of pressure, the numerical density errors, due to the convectional source term, generated in the previous time steps do not affect the source term. However, the previously accumulated velocity or position errors can still affect the source term.

Generally, in free surface problems an initial free surface particle can separate from the surface and becomes an inner particle below the surface. Also an inner particle can move to free surface when free surface extends. In convectional I-SPH the source term of (right-hand side of Eq. (15)) is considered for setting density of particles to their initial values. Initial value for density of free surface particles is smaller than that for inner particles. Therefore, significant density errors in the source term may occur due to imposing the incompressibility condition on free surface particles, using Eq. (15), because some of the particles on free surface may become inner ones and some of the inner particles may, later, become free surface ones. Using a source term for considering this matter is essential. The new source term proposed in this work, Eq. (31), considers this property and enhances both accuracy and stability of I-SPH method especially when the number of free surface and inner particles changes significantly in time.

In order to assess the improvements due to the imposed modifications, the dam-break problem is solved again using the modified incompressible SPH (M-I-SPH) method. The smooth shape of the free surface and the well agreement with the experimental results of Koshizuka and Oka (1996) in simulating the water column collapse (Fig. 6), proves the efficiency improvement of the modified form of I-SPH method.

In the dam-break problem simulation, the collapsing water runs on the bottom wall at 0.2 s. Accelerated water impinges the right vertical wall and rises up at 0.3 s. At 0.4 s, the water goes up losing its momentum and at $t = 0.5$ s it begins to come down. A mushroom shape is clear at $t = 0.7$ s and the waves fall down in the remaining water at $t = 0.8$ s. Around $t = 1$ s the main water reaches the left wall again. The computed motion of leading edge is compared with the experimental data (Koshizuka and Oka, 1996; Martin and Moyce, 1952) and is shown in Fig. 7. From this figure it can be clearly observed that the speeds of the leading edge obtained from experiments are slower than those of the calculations. This might be due to the friction between the fluid and the bottom wall that is neglected in the calculations.

Parameters used in the current model are investigated with test calculations of the collapse of a water column. β is the free surface parameter that is used to judge whether the particle is on the free surface or not. Fig. 8 shows the number of particles considered as the free surface using different free surface parameter (β). The trajectories are almost the same from $\beta = 0.8$ to 0.99, although they are shifted lower in parallel when the parameter is smaller. In this range of β values no instability in computation is observed. We can conclude that the free surface parameter is not effective to the calculation result if the calculation proceeds stably. In this paper $\beta = 0.95$ has been chosen.

Similar analyses have been performed in order to obtain the smoothing length or kernel range (h) (Fig. 9). The results of this analysis clearly show that using free surface parameter $\beta = 0.95$ and the smoothing length or kernel range of $h = 1.2 * L_0$, the number of free surface particles at the start of simulation is appropriate and will change smoothly over time. Thus, $h = 1.2 * L_0$ has been selected as the kernel range in this study because of lower computational cost.

The pressure filed of the problem at different times for the case with $\beta = 0.8$ is presented in Fig. 10, showing again that the results are not sensitive to this parameter (β). At $t = 0.1$ s the maximum pressure is about 1975 Pa at the left corner while the hydrostatic pressure is about 2430 Pa given by the weight of the liquid acting on a unit area at the water depth at the corner. After the initial large acceleration phase the velocity gradually becomes stable causing that pressure is almost hydrostatic. At $t = 0.3$ s, the water strongly hits on the right wall and the pressure at the right corner reaches about 4500 Pa while the hydrostatic is about 735 Pa, showing significant pressure deviation from the hydrostatic distribution. At $t = 0.7$ s the water goes up and at the corner the velocity is approximately zero causing hydrostatic pressure distribution properly simulated by the present method. At $t = 0.8$ s the water falls down and hits the bottom and again the pressure around $x = 0.3$ m deviates from hydrostatic distribution and reaches

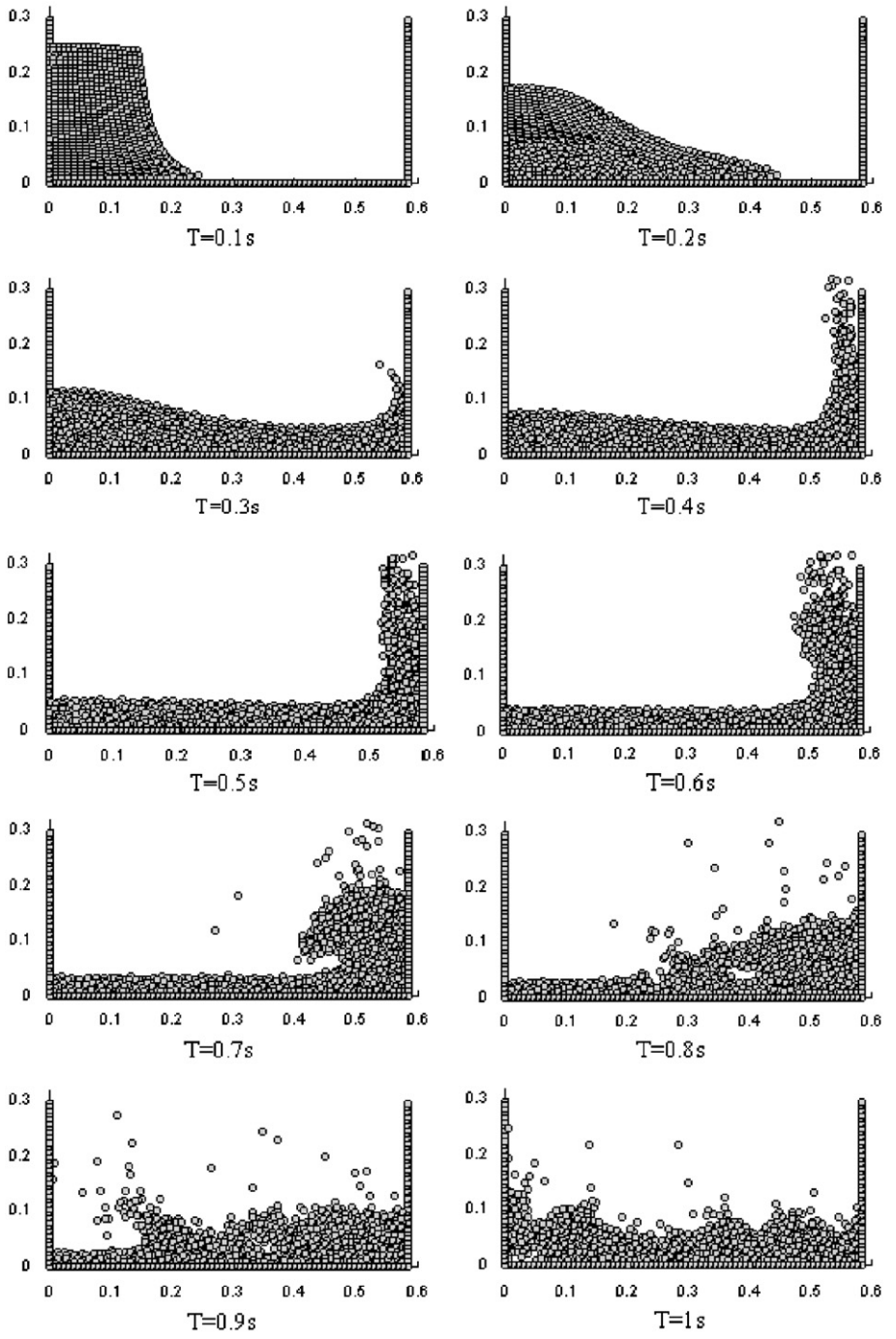

Fig. 6. Numerical simulation of collapse of water column at different times using M-I-SPH method (horizontal and vertical scales units are meter).

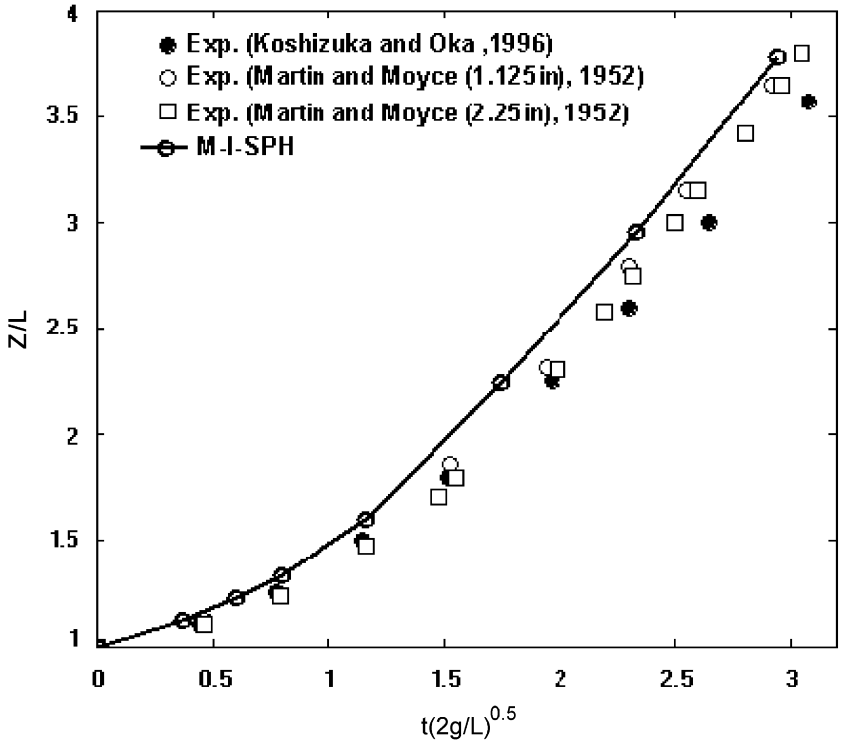

Fig. 7. Comparison between calculated motion of leading edge and the experimental data.

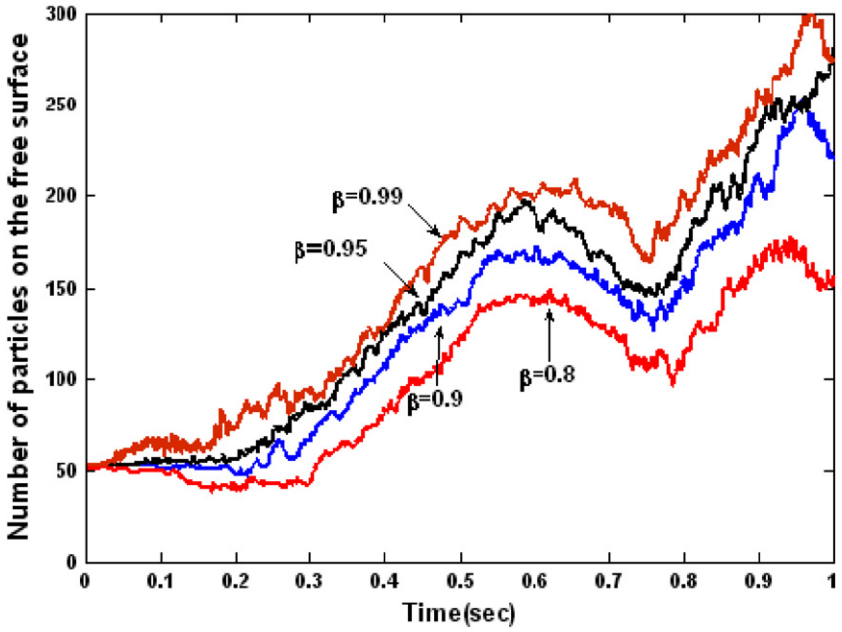

Fig. 8. Effect of free surface parameter (β) on the number of particles on the free surface ($h = 1.2L_0$).

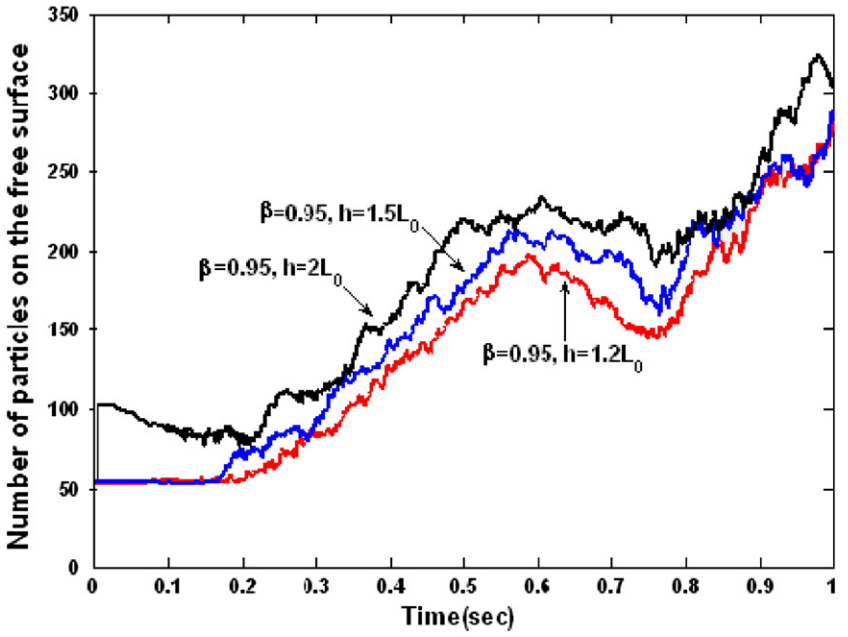

Fig. 9. Effect of smoothing length (h) on the number of particles on the free surface ($\beta = 0.95$).

about 1500 Pa. In Fig. 11, the velocity filed at different times is presented. At $t = 0.1$ s the velocities of the particles are approximately low especially at the corner. At $t = 0.3$ s since the water hits on the wall, the velocities are very high. At $t = 0.7$ s the velocities diminish and at $t = 0.8$ s again the velocities near $x = 0.3$ m are high.

Satisfying incompressibility condition provides an appropriate self-check on the accuracy of incompressible numerical models. For I-SPH and M-I-SPH models proposed in the paper, a quantitative measurement of the conservation of mass at each time step is provided by Eq. (31):

$$abs\left(\frac{\mathrm{d}\rho}{\mathrm{d}t}\right) = \sum_{a=1}^{N}\sum_{b} abs(m_b(\vec{u}_a - \vec{u}_b)\cdot\vec{\nabla}_a W_{ab}), \tag{33}$$

where N is the number of fluid particles used in Eq. (33) .

If incompressibility is satisfied for all particles, the density changes of all particles ($abs(\mathrm{d}\rho/\mathrm{d}t)$) are zero at each time step. In order to show the ability of the M-I-SPH method to satisfy incompressibility of free surface particles, density changes of inner fluid and all particles including free surface and inner particles have been recorded for both method of I-SPH and M-I-SPH till 1 s as shown in Fig. 12. Density errors of all particles in Eq. (33) are more than density errors of inner particles using I-SPH, showing that I-SPH method does not satisfy incompressibility of free surface particles well especially after the water hits the wall. In the figure also density errors of all and only inner particles are compared and clearly shows that M-I-SPH much better satisfy incompressibility of free surface particles than I-SPH because of employing the modified pressure Poisson equation (24) on surface particles. The most important point which is visible in the figure is that M-I-SPH method much better satisfies incompressibility condition of both free

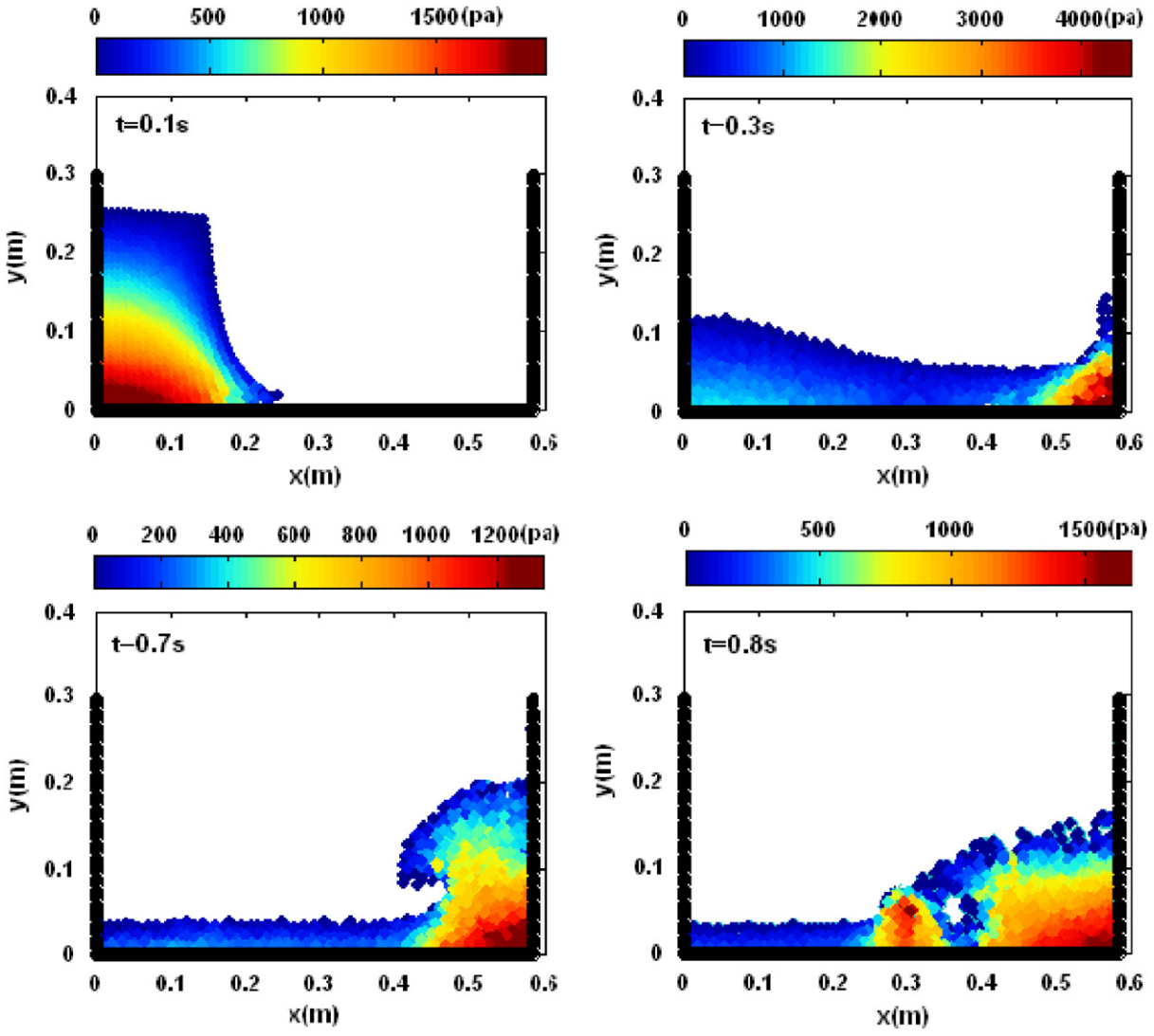

Fig. 10. Pressure field of the dam-break problem computed by M-I-SPH at different times ($\beta = 0.8$).

surface and inner particles due to using the proposed modifications (imposing directly incompressibility of surface particles and the new source term of Eq. (31). For example density error for I-SPH at $t = 1$ s is about 2% but for M-I-SPH is about 0.5% indicating the ability of the modification to satisfy mass conservation.

6.2. *Evolution of an elliptical water bubble*

Simulating the evolution of an elliptic water bubble in 2-D is another simple test for verification of the presented M-I-SPH formulations. The velocity field is linear in the coordinates and is expressed by the

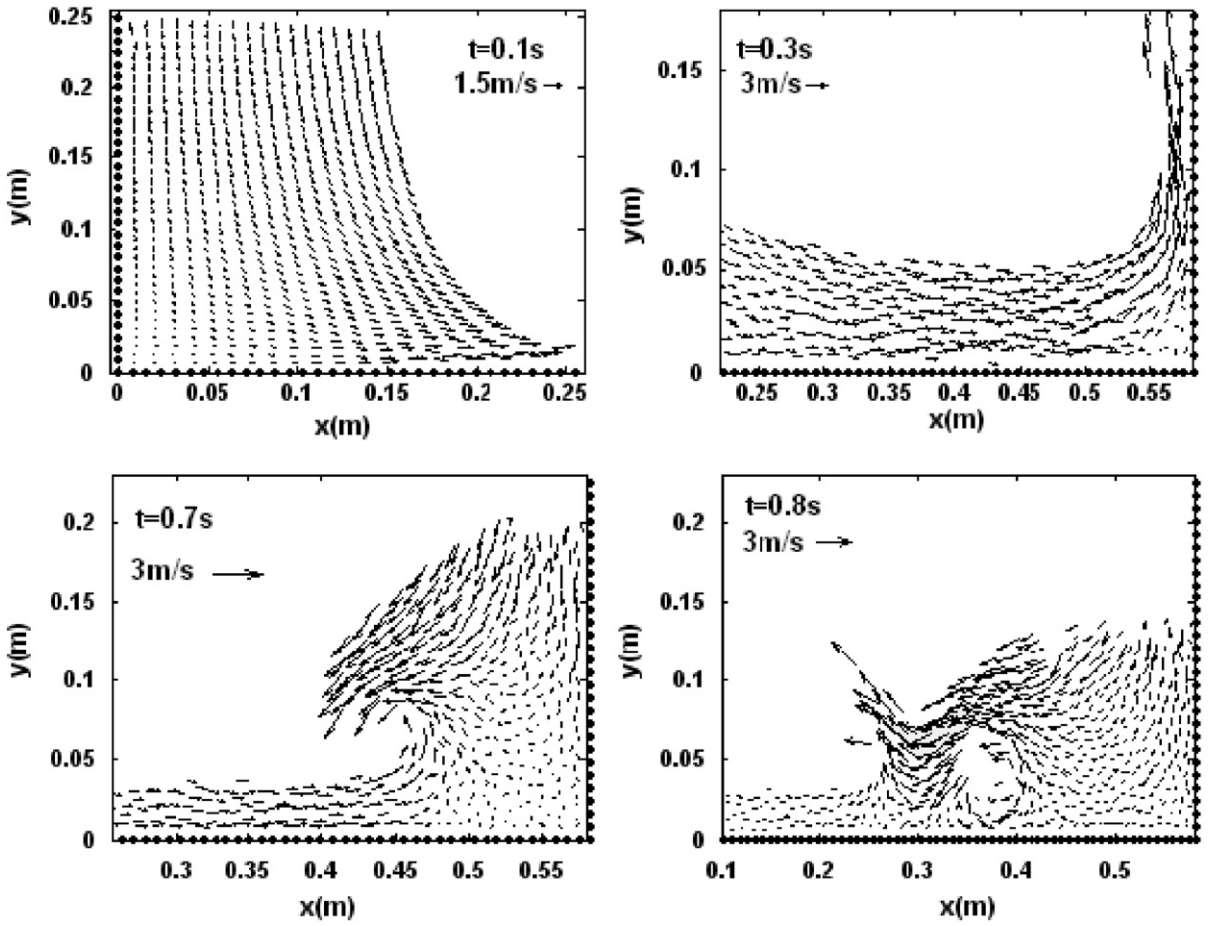

Fig. 11. Velocity field of the dam-break problem computed by M-I-SPH at different times ($\beta = 0.8$).

following equation:

$$V = (-100x; 100y). \tag{34}$$

This problem is studied on two axis (a, b) and the initial configuration of particles is a unit circle. The initial particle spacing $L_0 = 0.05$ m (1273 particles) and the constant time step $\Delta t = 10^{-5}$ s were employed in the computations. The numerical results of simulation of the evolution of water bubble over time are shown in Fig. 13 using both M-I-SPH and I-SPH methods. The shapes of the water bubble simulated by M-I-SPH are more rounded especially at large times indicating the ability of the present method compared with the convectional one.

The evolution of an elliptic water bubble can also be solved in an analytical way (Monaghan, 1994). The theoretical values of semi-major axis (b) of the drop at different times and the values computed by M-I-SPH method and the I-SPH method are shown in Table 1. The computation errors of M-I-SPH method are less than 2.5% while they are less than 4% when I-SPH method is used. The decrease in

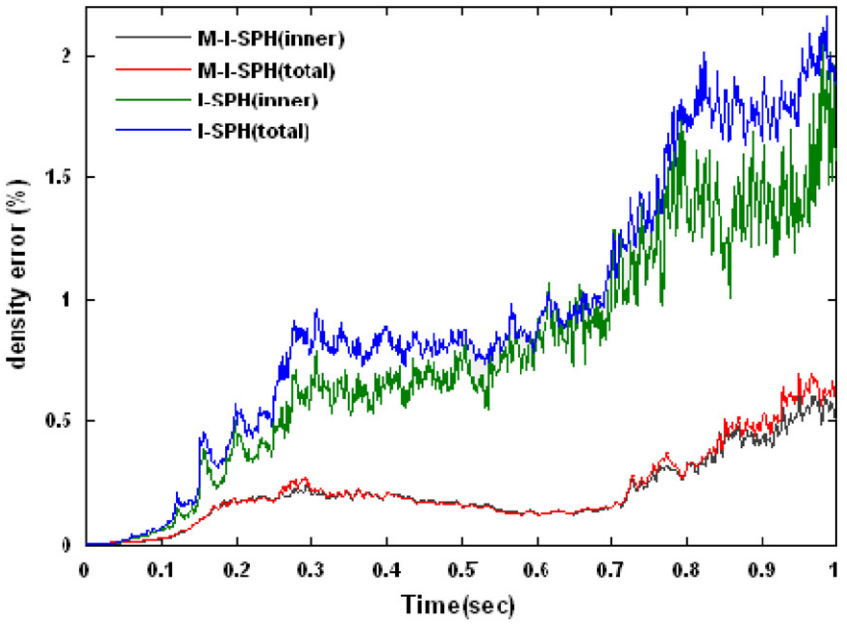

Fig. 12. Comparison between density errors for I-SPH and M-I-SPH methods.

computation errors using M-I-SPH method, again, proves the improvement in the result obtained by the M-I-SPH method.

The vertical velocity of particles along the major axis of the drop at time $t = 0.008$ s using M-I-SPH method, are compared with the related analytical solution values in Fig. 14. As clearly observed in the figure, there is an excellent agreement between the numerical and analytical results.

6.3. Solitary wave breaking on a mild slope

The laboratory breaking solitary wave experiment of Synolakis (1986) is used as another convincing test to show the capability of the M-I-SPH method. In the experiment the still water depth was $d = 0.21$ m, the slope of the beach was $s_0 = 1:20$ and the incident wave height was $a/d = 0.28$. The initial particle spacing is $L_0 = 0.0191$ m and totally about 2700 particles are used in the simulations. The computational domain started from the front of the foot of the slope and extended to the location beyond the maximum run-up point. The initial solitary wave profile was produced according to Monaghan and Kos (1999). The initial vertical velocity of all particles at the initial conditions is set to zero and the horizontal velocities are assigned based on the Boussinesq equation (Lo and Shao, 2002). The computed wave profiles by the present method are shown in Fig. 15. The good agreement between the computed and experimental wave profiles demonstrates the capability of the M-I-SPH method again. The maximum run-up height computed by the present method is about 0.52d which is close to 0.48d reported by Lin et al. (1999) using RANS calculation but the experimental run-up height is about 0.42d Synolakis (1986). This upper prediction of the maximum run-up might be due to neglecting of the viscosity term in the momentum equation. The same problem has been solved by Lo and Shao (2002) by I-SPH method. They used about 10 000 particles in their computations. In spite of fewer particles used in the present method (2700 particles) and

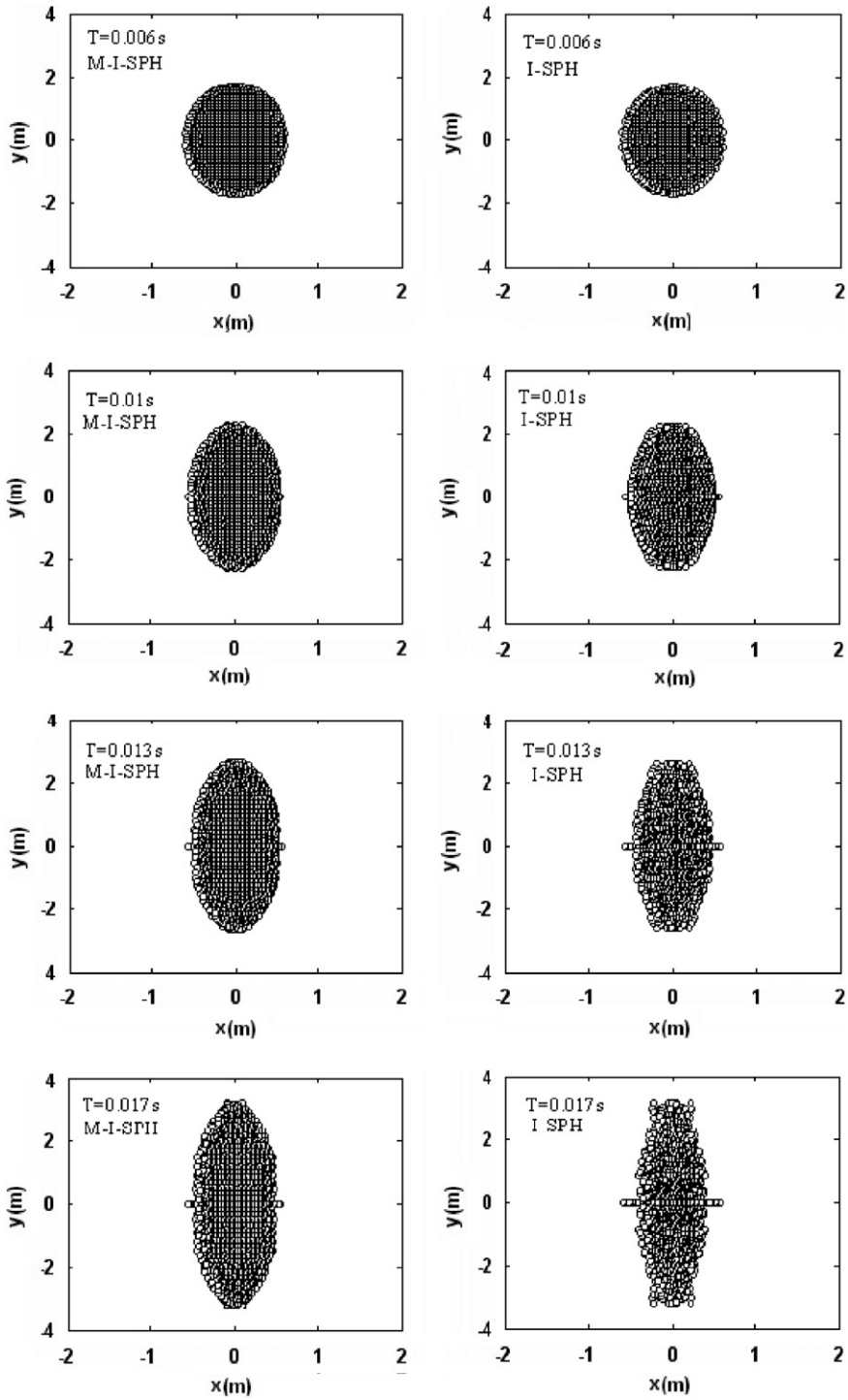

Fig. 13. Comparison between particle configurations for the evolution of an elliptical drop using M-I-SPH and I-SPH methods.

Table 1
Comparing theoretical values of b (semi-major axis) of the elliptical drop with computed values of modified incompressible SPH method and incompressible SPH method

Time (s)	Theoretical value (m)	Modified incompressible SPH method		Incompressible SPH method	
		Computed value (m)	% error	Computed value (m)	% error
0.005	1.595	1.591	0.251	1.59	0.313
0.007	1.863	1.854	0.483	1.845	0.966
0.01	2.277	2.25	1.186	2.235	1.845
0.012	2.56	2.517	1.680	2.496	2.500
0.015	2.977	2.913	2.150	2.886	3.057
0.018	3.4	3.32	2.353	3.28	3.529

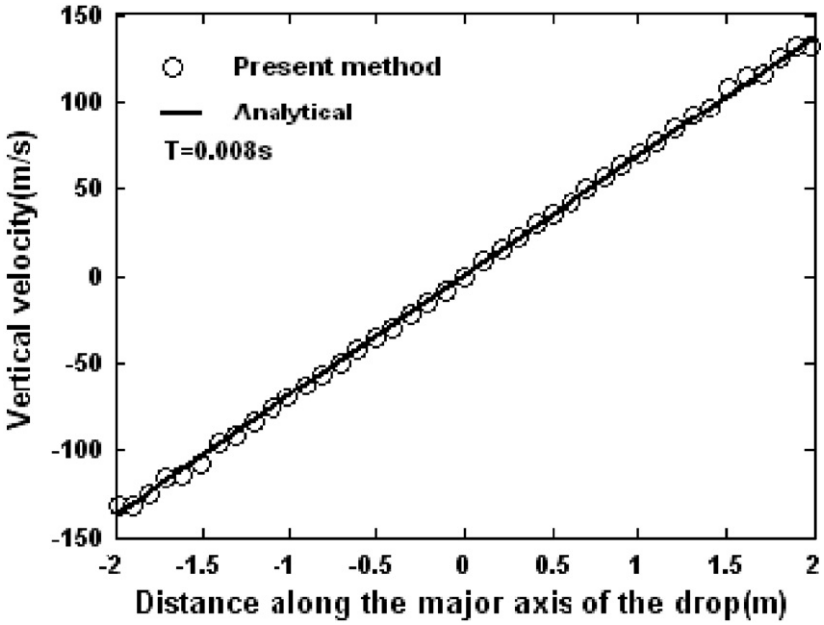

Fig. 14. Comparison between simulated and analytical solutions of vertical velocity of the drop computed by M-I-SPH.

also neglecting of the viscosity term, the results are as good as theirs demonstrating the accuracy of the present method.

6.4. Tsunami run-up

In the previous section, propagation and run-up of a breaking wave on a mild slope was investigated. In this section run-up of non-breaking waves on a steep slope is studied. These waves can propagate shoreward and damage coastal structures. Estimating the flooding area of the coastal zone caused by

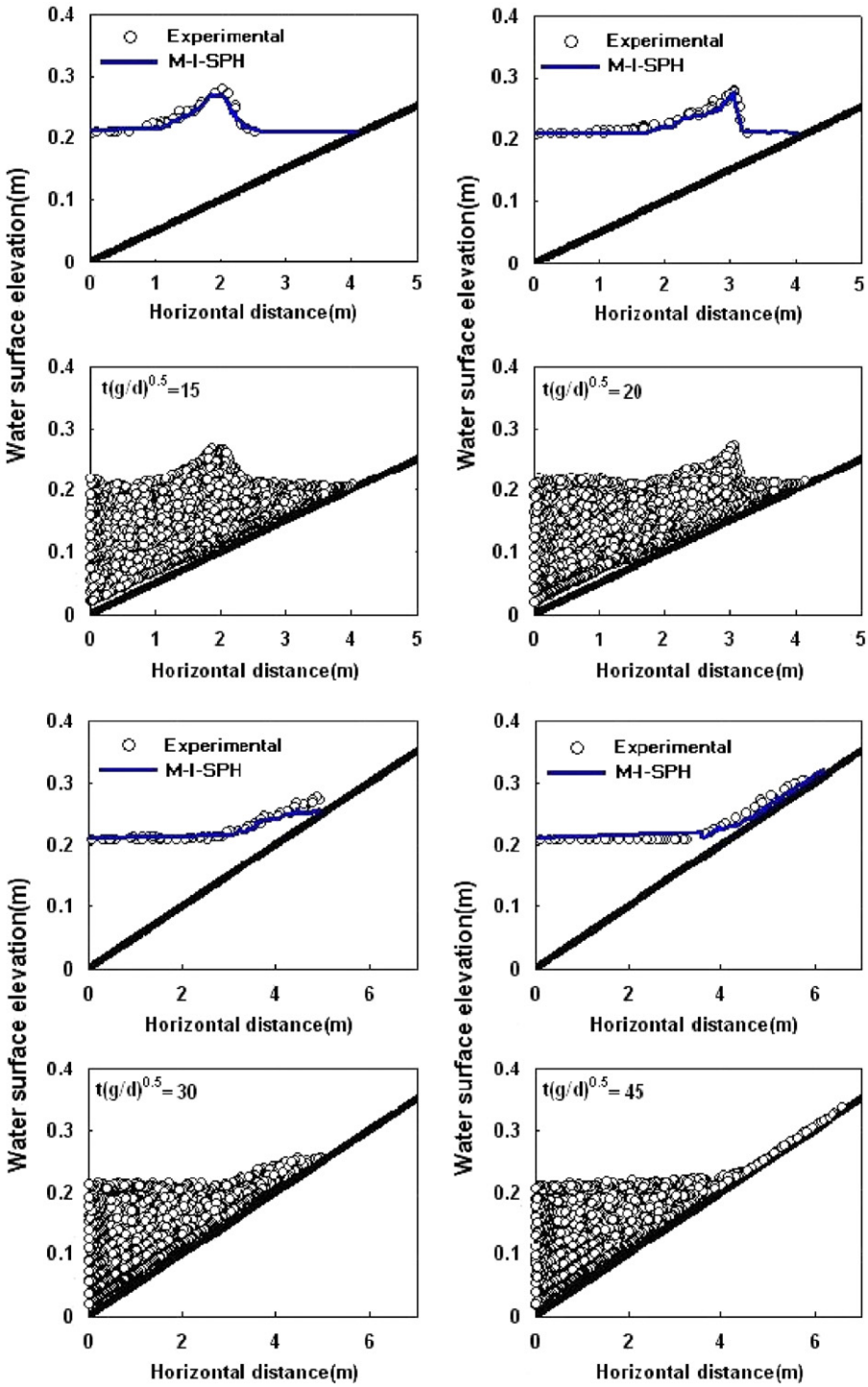

Fig. 15. Particle configurations and comparison of values computed by M-I-SPH and experimental surface profiles of solitary wave.

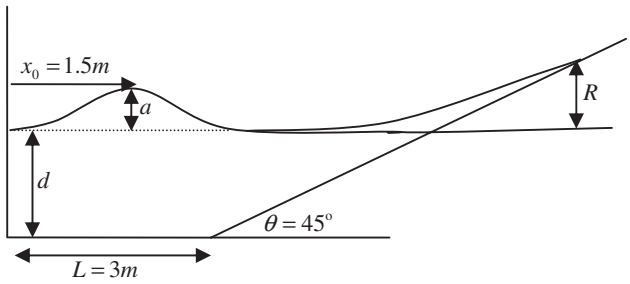

Fig. 16. Geometry of the tsunami run-up problem.

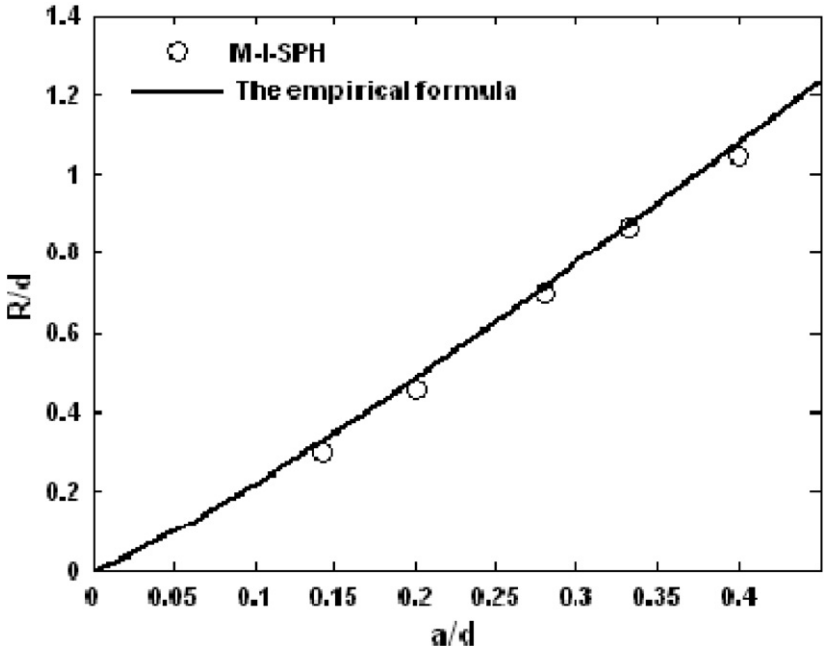

Fig. 17. Comparison between tsunami run-ups computed by M-I-SPH and the empirical formula.

tsunami waves is essential for tsunami hazard mitigation (Gedik et al., 2005). In order to determine run-up of long waves, different theoretical and experimental studies have been performed such as the experimental work reported by Hall and Watts (1953).

The Hall and Watts empirical formula for solitary wave run-up on an impermeable slope with $\alpha = 45°$ is

$$\frac{R}{d} = 3.1\left(\frac{a}{d}\right)^{1.15}, \tag{35}$$

where R is wave run-up height, d is the water depth and a is the wave height. In Fig. 16, these parameters and also the initial conditions for this problem are shown. The initial particle spacing $L_0 = 0.05$ m, the

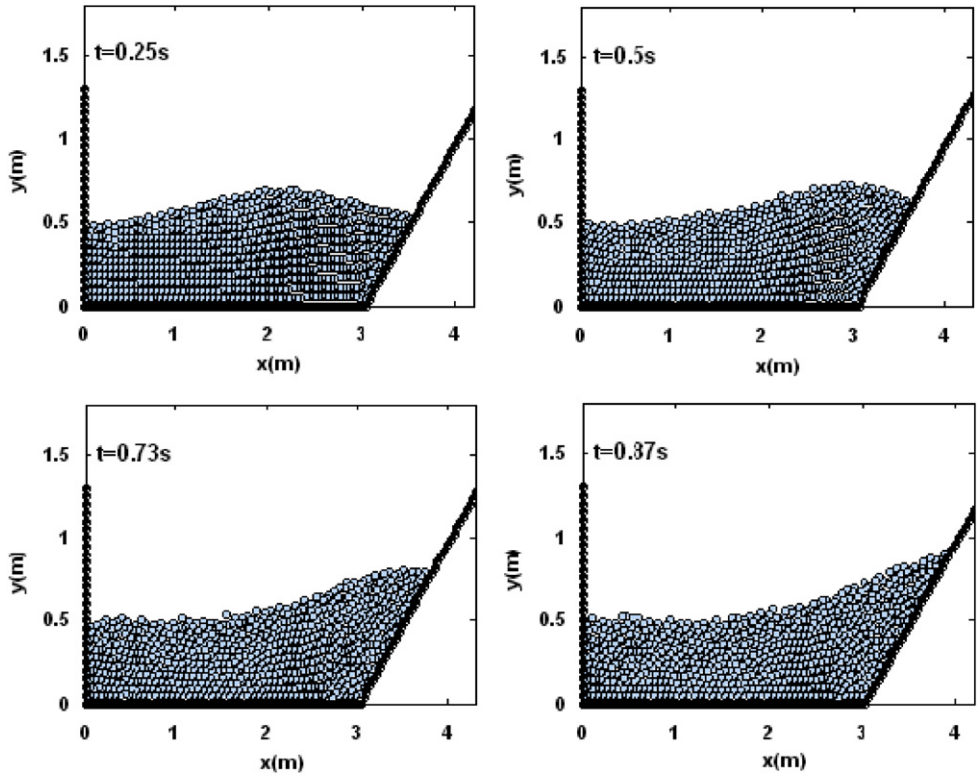

Fig. 18. Particle configurations at different times for tsunami run-up problem simulated by M-I-SPH method.

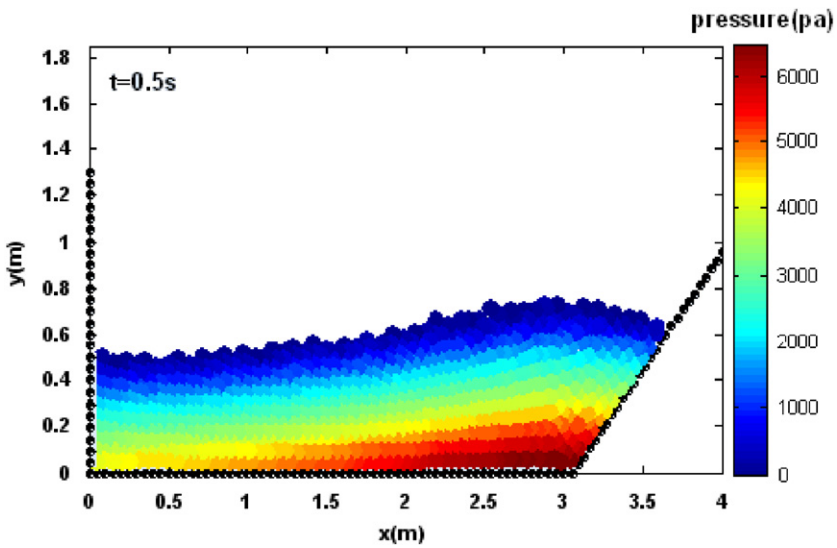

Fig. 19. Pressure field of tsunami run-up problem at $t = 0.5$ s ($a = 0.2$ m, $d = 0.5$ m) by M-I-SPH.

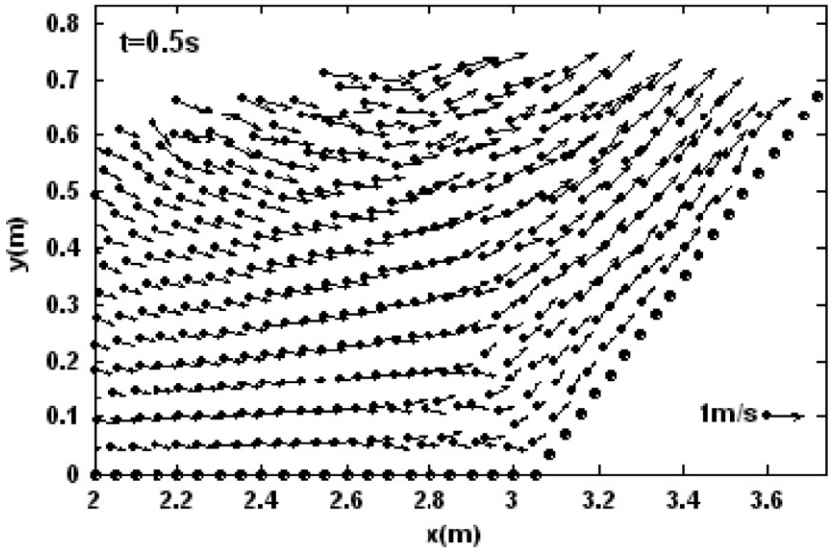

Fig. 20. Velocity field of tsunami run-up problem at $t = 0.5$ s ($a = 0.2$ m, $d = 0.5$ m) by M-I-SPH.

number of particles about 1150 and time step was controlled by $\Delta t \leqslant 0.1 L_0 / V_{\max}$. In this problem like the previous one, the initial solitary wave profile and horizontal velocities are assigned based on Boussinesq equation (Lo and Shao, 2002).

The problem was solved for five different cases of water depth and amplitude and for each, the run-up (R) has been recorded. In Fig. 17, the computed run-up and the empirical results (Eq. (35)) are compared. The good agreement between the computational results and experimental data demonstrates the ability of the present method to simulate run-up due to tsunami waves.

In Fig. 18, the particle configurations for the case with $a = 0.2$ m, $d = 0.5$ m at different times are shown. The figure illustrates propagation of the non-breaking wave toward the slope. It should be noted that because of steepness of the slope, wave breaking does not occur. In Fig. 19, the computed pressure field for this case at $t = 0.5$ s is shown. It is clear that the pressure of the particles located far from the slope is almost hydrostatic which is due to the approximately zero velocity of these particles and also in Fig. 20, the velocity field of the problem at $t = 0.5$ s is presented. Velocities of the particles on the slope and free surface are higher than those of the other particles.

7. Conclusion

A modified formulation of I-SPH method is introduced and applied to simulate incompressible flows with free surface. In this method grids are not necessary and particles are used to simulate the flow. Thus because of the Lagrangian nature of this method, numerical diffusion error that is due to the advection term of N-S equations does not arise. Using a new form of source term for the Poisson equation of pressure and enforcing incompressibility to free surface particles, stability and accuracy of the conventional I-SPH method are improved. The M-I-SPH method was applied to model dam-break flow, evolution of an elliptic water bubble, solitary wave breaking on a mild slope and run-up of non-breaking waves on steep slopes.

The satisfactory results obtained by the present method prove the ability of the M-I-SPH to simulate a wide range of fluid mechanics problems.

References

Ataie-Ashtiani, B., Farhadi, L., 2006. A stable moving-particle semi-implicit method for free surface flows. Fluid Dyn. Res. 38 (4), 241–256.

Ataie-Ashtiani, B., Shobeiry, G., 2008. Numerical simulation of landslide impulsive waves by Smooth Particle Hydrodynamics. Int. J. Numer. Meth. Fluids 56 (2), 209–232.

Farhadi, L., Ataie-Ashtiani, B. 2004a. Improved MPS method for simulating water flow with irregular free surface. In: XV International Conference on Computational Methods in Water Resources, Chapel-Hill, USA, June 13–27, pp. 1743–53.

Farhadi, L., Ataie-Ashtiani, B. 2004b. A fully mesh-less Lagrangian numerical method for prediction of free water surface. In: International Conference on Hydraulics of Dams & River Structures, Tehran, Iran, April 26–28, pp. 345–352.

Gedik, N., Irtema, E., Kabdaslib, S., 2005. Laboratory investigation on tsunami run-up. Ocean Eng. 32, 513–528.

Gingold, R.A., Monaghan, J.J., 1977. Smoothed particle hydrodynamics: theory and application to non spherical stars. Mon. Not. R. Astron. Soc. 181, 375–389.

Gomez-Gesteria, M., Dalrymple, R., 2004. Using a three-dimensional smoothed particle hydrodynamics method for wave impact on a tall structure. J. Waterw. Port. Coastal Eng. 130 (2), 63–69.

Hall, J.V., Watts, J.W. 1953. Laboratory investigation of the vertical rise of solitary waves on impermeable slopes. Technical Memorandum 33, Beach Erosion Board, Office of the Chief of Engineers, U.S. Army Corps of Engineers.

Harlow, F.H., Welch, J.E., 1965. Numerical calculation of time-dependent viscous incompressible flow of fluid with free surface. J. Phys. Fluids. 8 (12), 322–329.

Hirt, C.W., Nichols, B.D., 1981. Volume of fluid (VOF) method for the dynamics of free boundaries. J. Comput. Phys. 39, 201–225.

Koshizuka, S., Oka, Y., 1996. Moving-particle semi-implicit method for fragmentation of incompressible fluid. J. Nucl. Sci. Eng. 123, 421–434.

Koshizuka, S., Nobe, A., Oka, Y., 1998. Numerical analysis of breaking waves using the moving particle semi-implicit method. Int. J. Numer. Meth. Fluids 26, 751–769.

Koshizuka, S., Ikeda, H., Oka, Y., 1999. Numerical analysis of fragmentation mechanisms in vapor explosion. Nucl. Eng. Des. 189, 423–433.

Lin, P.Z., Chang, K.A., Philip, L.F., 1999. Runup and rundown of solitary waves on sloping beaches. J. Waterw. Port. Coastal Ocean Eng. ASCE 125 (5), 247–255.

Liu, G.R., 2003. Mesh Free Methods: Moving Beyond the Finite Element Method. Chemical Rubber, Boca Raton, FL.

Lo, E.Y.M., Shao, S.D., 2002. Simulation of near-shore solitary wave mechanics by an incompressible SPH method. Appl. Ocean Res. 24, 275–286.

Martin, J.C., Moyce, W.J., 1952. An experimental study of the collapse of liquid columns on a rigid horizontal plane. Philos. Trans. R. Soc. London Ser. A 244, 312–324.

Monaghan, J.J., 1992. Smoothed particle hydrodynamics. Annu. Rev. Astron. Astrophys. 30, 543–574.

Monaghan, J.J., 1994. Simulating free surface flows with SPH. J. Comput. Phys. 110, 399–406.

Monaghan, J.J., 1996. Gravity currents and solitary waves. Physica D 98, 523–533.

Monaghan, J.J., Kos, A., 1999. Solitary waves on a Cretan beach. J. Waterw. Port. Coastal Ocean Eng. 125 (3), 145–154.

Shao, S.D., Gotoh, H., 2005. Turbulence particle models for tracking free surfaces. J. Hydraul. Res. 43 (3), 276–289.

Shao, S.D., Lo, E.Y.M., 2003. Incompressible SPH method for simulating Newtonian and non-Newtonian flows with a free surface. Adv. Water Resour. 26 (7), 787–800.

Synolakis, C.E. 1986. The run-up of long waves. Ph.D. Thesis, California Institute of Technology, Pasadena, CA, USA.

Sussman, M., 2003. A second order coupled level set and volume-of-fluid method for computing growth and collapse of vapor bubbles. J. Comput. Phys. 187, 110–136.